Catalysis Today 168 (2011) 38–47

Contents lists available at ScienceDirect

Catalysis Today

journal homepage: www.elsevier.com/locate/cattod

How defects and crystal morphology control the effects of desilication

Stian Svelle[a,*], Linn Sommer[a], Katia Barbera[b], Peter N.R. Vennestrøm[c,d], Unni Olsbye[a], Karl Petter Lillerud[a], Silvia Bordiga[b], Ying-Hsi Pan[c], Pablo Beato[c,**]

[a] inGap Center for Research Based Innovation, Department of Chemistry, University of Oslo, P.O. Box 1033, Blindern, N-0315 Oslo, Norway
[b] Dipartimento di Chimica IFM-NIS Centre of Excellence, Universita di Torino, Via P. Giuria 7, 10125 Turin, Italy
[c] Haldor Topsøe, Nymøllevej 55, DK-2800 Kgs, Lyngby, Denmark
[d] Instituto de Tecnología Química, UPV, Av. Naranjos s/n, E-46022 Valencia, Spain

ARTICLE INFO

Article history:
Received 15 October 2010
Received in revised form
30 November 2010
Accepted 1 December 2010
Available online 26 January 2011

Keywords:
ZSM-5
Mesoporosity
Alkali treatment
Methanol to gasoline
Intergrowths

ABSTRACT

The introduction of mesoporosity in zeolites by desilication has become a simple routine method to generate hierarchical materials with improved catalytic performance. The mesopore formation upon alkali leaching has been investigated employing electron microscopy, infrared spectroscopy, temperature programmed desorption of ammonia, and a catalytic test reaction. We are able to demonstrate that the mesopores are formed by two modes. They are created both as a consequence of Al-directed dissolution of siliceous areas and selective dissolution or etching along boundaries, intergrowths, and defects within each particle are important. This has allowed us to identify a preferred particle morphology for efficient desilication. Particles constructed of fused subunits appear to be very susceptible towards directed mesopore formation by desilication. The desilication may also lead to alterations of the aluminum environment, seen as a reduction in the concentration of strong Brønsted sites and the appearance of a second family of weaker sites. Introduction of mesoporosity by carbon templating rather than desilication leads to a material with a more complex distribution of surface hydroxyl groups.

1. Introduction

Microporous zeolites have found widespread application in catalytic and separation processes within the refining and petrochemical industries, as recently reviewed by Vermeiren and Gilson [1]. The microporous nature of the zeolites, comprising pores and cavities of molecular dimensions, results in a high internal surface area and shape selective properties and is the major cause of such widespread application. However, it is the same microporosity that imposes constraints on the effective use of zeolites in many applications, primarily due to diffusion resistance experienced by bulky reactant molecules, which will lead to inefficient utilization of the internal catalytic surface, or in the most severe situation, the complete exclusion of reactants [2]. Such a situation is particularly pertinent for the catalytic cracking or hydrotreating/cracking of crude oil, which is becoming increasingly heavier. Several research strategies exist that might circumvent this limitation. Substantial progress has been reported for the synthesis of zeolites and related materials with extra large pores, *i.e.* pores with a circumference defined by more than 12 T-atoms [3]. However, the synthesis of such materials is not yet straightforward, and the hydrothermal stability might sometimes be an issue [4]. Easier access to the full internal surface might be gained by reducing the dimension of the crystallites by the synthesis of nanometer sized zeolite crystals [5], but this leads to other issues related to powder handling and processing. Another strategy is to introduce a second level of porosity comprising substantially larger pores, *i.e.* mesopores, leading to the creation of so-called hierarchical zeolites [6–8]. Again, several routes might be pursued in order to reach this goal, such as various templating techniques [9], or post synthesis treatments. Among the post synthesis treatments, desilication by dilute alkali leaching has been shown to be and efficient and relatively straightforward method by which to introduce mesoporosity into zeolite crystals and has quickly become a routine method.

Early systematic studies of desilication methods were performed by Le Van Mao et al., who observed selective silicon removal from zeolite frameworks after leaching with sodium carbonate solutions [10]. In further works, the adjustment of the pH by adding sodium hydroxide in order to control the desilication process was explored [11,12]. Ogura et al. reported improved catalytic properties after alkali treatment with NaOH and attributed their observations to enhanced diffusion properties within the material due to mesoporosity [13,14]. The advantage of leaving the catalytically active sites largely unaffected together with the simplicity of the method led to more systematic investigations of the desilication method, especially by Groen et al. for the case of zeolite ZSM-5

* Corresponding author. Tel.: +47 22 85 54 54; fax: +47 22 85 54 41.
** Corresponding author. Tel.: +45 45 27 20 00; fax: +45 45 27 29 99.
E-mail addresses: stian.svelle@kjemi.uio.no (S. Svelle), pabb@topsoe.dk (P. Beato).

0920-5861/$ – see front matter © 2010 Elsevier B.V. All rights reserved.
doi:10.1016/j.cattod.2010.12.013

[15–21]. However, also the transferability of the method to other zeolite topologies has been studied [22]. Today, studies on the effect of desilication on a variety of zeolite topologies have been reported [23–32]. Whereas the first studies were primarily concerned with the introduction and characterization of mesoporosity, the catalytic properties of many of the obtained materials are also reported [13,23–26,33–36]. Recently, also protocols with other desilication agents than NaOH and Na_2CO_3 have been developed [37–39]. Even so, by far the most extensive investigations concerned with the influence of treatment parameters on the mesopore formation have been made for zeolite ZSM-5. The influence of parameters like concentration of the alkaline solution, temperature and exposure time and the general susceptibility towards alkali leaching may vary from topology to topology, but some principles seem to be quite universally applicable.

The underlying *mechanism* of mesopore formation is based on the hydrolysis of Si–O–Si and Si–O–Al bonds in alkaline medium. The hydroxide anions (OH^-) can attack the zeolite framework at defect sites, namely silanol groups. The expelled silicate anion is stabilized by the accompanying alkali cation, leaving a vacancy in the framework. When comparing different counter ions, the best effect was found for NaOH due to its superior capability to stabilize silicate anions [21]. However, the *mode* of mesopore formation, concerning *e.g.* where and to which extent each zeolite particle is attacked by the alkaline solution, is more elusive. Two main proposals appear in the literature, *i.e.* mesopore formation by the dissolution of siliceous areas defined by surrounding and more persistent Al tetrahedra and mesopore formation along internal crystallite boundaries caused by twinning and other intergrowth phenomena.

Ciziek et al. found an important correlation between the Al content of the material and its susceptibility towards desilication. Repulsion between the negatively charged AlO_4 tetrahedra and OH^- was suggested to hamper the hydrolysis of Si–O–Al bonds compared to the hydrolysis of Si–O–Si bonds and hence, Al has a moderating influence on the dissolution rate of the material [40]. However, the study of Ciziek et al. was not concerned with mesopore formation, but with non-directed dissolution of MFI crystals. The importance of the Al content for the controlled generation of mesoporosity has been made exceedingly clear by the detailed studies of Groen et al. for zeolite ZSM-5 [16,18,19,21]. They demonstrated that an initial Si/Al ratio of 25–50 is most favorable for the controlled desilication of the zeolites ZSM-5, mordenite and ZSM-12 [16,23,27]. At lower Si/Al ratios, the mesopore formation is limited by the repulsion between OH^- and the negatively charged lattice, whereas higher Si/Al ratios open up for extensive mesopore formation accompanied by a severe loss of crystallinity [16]. For other topologies, as also pointed out by Pérez-Ramírez et al. in addition to the initial Si/Al ratio, the stability of framework Al within the respective zeolite topology is crucial to the formation of mesoporosity [7]. In the case of *e.g.* zeolite beta, the treatment with alkaline solutions leads to the dissolution of the framework without preserving the catalytically important Brønsted acid sites [24]. Low framework Al stability has also been found to be problematic for the desilication of zeolite SSZ-13 [30].

Ogura et al. proposed that mesopores are formed along boundaries of ZSM-5 crystallite twinning, which were suggested to have a poor resistance against alkaline media [41]. This kind of disorder, linear, two-dimensional and macro-defects have been studied extensively, however, mostly in other respects. Structural disorder and stacking faults may *e.g.* cause an interruption of the zeolite three-dimensional pore system, and as a consequence, parts of the pore system might be unavailable, making parts of the crystal ineffective in catalysis. For example, the diffusion rates of toluene were found to be 3 magnitudes lower in polycrystalline ZSM-5 than in a single crystal [42]. In the course of diffusion studies, and recently also in connection with catalysis, attention has been paid to the investigation of intergrowth boundaries in zeolites [43–48]. Traditionally, defects like stacking faults and the intergrowth of different crystal structures in zeolites have been investigated by electron microscopy and atomic force microscopy [49–52]. Not only intergrowth of two different zeolite structures can be observed, but also intergrowth of structural subunits. In large crystals, these intergrowth boundaries become visible in optical microscopy when etching and/or coloring dyes are applied [53]. Very recently, Weckhuysen and co-workers and Roeffaers et al. developed confocal fluorescence microscopy setups that allow both the investigation of intergrowth structures and the mapping of catalytic activity in individual zeolite crystals [48,54–57].

In this work, we have studied the mode of mesopore formation after desilication of several ZSM-5 samples using predominantly electron microscopy (TEM and SEM), in addition to the regular array of characterization techniques. We clearly observe mesopore formation according to both suggestions summarized above. The dissolution of certain areas (possibly siliceous) leading to "holes" in the particles is clearly observable. In addition, we find mesoporous "superhighways" that appear to have been formed along crystallite intergrowth boundaries. These observations allow us to identify preferred crystal morphology for efficient desilication, and it appears that effects of crystal size are subsidiary to the effects of morphology. We also report on the changes in acidic and consequently catalytic properties upon desilication, as investigated using Fourier transformed infrared spectroscopy (FTIR), temperature programmed desorption of ammonia (NH_3-TPD-TGA), and catalyst performance in the methanol to hydrocarbons (MTH) reaction. Moreover, we compare mesopore formation by desilication to the alternative route of carbon templating, in particular with respect to the concentration and nature of the surface defects.

2. Experimental

2.1. Catalyst preparation

A commercially available H-ZSM-5 from Zeochem International (PZ-2/100H, stated Si/Al ratio 50) was used and is referred to as *c*-ZSM-5 (*c* = commercial), while its desilicated counterpart has been named *c*-ZSM-5-*at* (*at* = alkali treated). Three samples were synthesized in the lab: one sample with comparable characteristics to the commercial sample (*h*-ZSM-5, *h* = home made), one sample consisting of similar morphology as the former but with large crystal size (*h*-ZSM-5-*xl*, *xl* = large crystals) and one carbon templated mesoporous sample (*h*-ZSM-5-*ct*, *ct* = *carbon templated*).

The *h*-ZSM-5 sample was synthesized by slowly adding 0.95 g of $NaAlO_2$ to a mixture of 119.14 g tetrapropylammonium hydroxide in 138 mL of deionized H_2O, while stirred in an ice-bath. To this mixture first 119.13 g of Ludox® TMA and then 22.7 g of sodium silicate were added. The mixture was further stirred for 15 h, while the temperature reached ambient temperature. The resulting gel was transferred into a Teflon® lined stainless steel autoclave and heated for 48 h at 423 K. The product was recovered by filtration and washed three times with water. After drying at 383 K, the sample was calcined in air to 823 K for 8 h. The acidic form of the desilicated zeolite was produced by two consecutive ion exchanges with a buffer solution of 1.7 M NH_4NO_3/0.94 M NH_3, using 10 mL solution per gram catalyst, at 353 K under stirring for 2 h. After each exchange, the NH_4-form of the zeolites were filtered, washed with water, and dried in air at 383 K. The final H-form of the parent zeolite and desilicated zeolite were obtained by heating the NH_4-form in air to 823 K for 3 h.

The *h*-ZSM-5-*xl* was prepared from a solution of 1254 g sodium silicate (27.7% SiO_2, 8.2% Na_2O, Borup Kemi) with 726 g deionized water and another solution of 156 g tetrapropylammonium bromide (98% Aldrich), 44 g aluminum sulphate octadecahydrate (Sigma–Aldrich > 99%), 104.9 g sulfuric acid (96%) and 660 g deionized water. A detailed synthesis procedure is given in another contribution in this issue [58].

The desilication procedure for the materials discussed in this study was as follows: the starting materials were treated with a 0.3 M NaOH solution (33 mL solution per gram catalyst material) for 30 min at 343 K, followed by cooling in an ice-bath to stop the desilication, and then washed three times with water by centrifugation. The *h*-ZSM-5-*xl*-*at*, was prepared in a similar manner; the material was treated by 30 mL solution per gram catalyst material at 338 K for 60 min. The desilicated ZSM-5 was dried over night at room temperature before further treatment. The acidic form of the desilicated zeolites was produced by the same ion-exchange procedure as described above for *h*-ZSM-5.

For the synthesis of carbon templated mesoporous zeolites, carbon black particles (BP-2000) having an average particle diameter of 12 nm, obtained from Carbot Corporation, was used as inert matrices. Carbon black was dried at 383 K for 24 h prior to use and then impregnated to incipient wetness, using aluminum isopropoxide as aluminum source. A detailed description of the synthesis procedure has been described in [59]. The composition of the final synthesis gel was: $1Al_2O_3$:80 SiO_2:50 TPA_2O:$1Na_2O$:1600·H_2O.

2.2. Catalyst characterization

TEM investigations were carried out using an FEI CM200 FEG-TEM operating at 200 kV. TEM specimens were prepared by crushing some specimen powder in a mortar and dispersing the powder in ethanol. The suspension was then drop-cast onto a 200 mesh copper grid covered with a lacy carbon film. The grids were dried in air at room temperature.

SEM work was done on a FEI XL30 FEG-SEM operating at 5–15 kV. SEM specimens were prepared by placing a small amount of sample powder on carbon tape on SEM stubs. In order to minimize the charging issue, the samples were coated with ca. 12 nm thick Pd/Pt layer.

Nitrogen physisorption was performed at 77 K using a Micromeritics ASAP 2020 instrument. All samples were outgassed in vacuum at 573 K for 16 h prior to measurements.

The acid site density of the materials was determined by temperature programmed desorption of ammonia (NH_3-TPD). The TPD profiles were monitored by thermogravimetric analysis (TGA), using a Mettler TG/DSC1 LF instrument. Between 40 and 60 mg sample was dried in N_2 at 773 K for 2 h in a TGA crucible, and cooled to 423 K. Ammonia was adsorbed at that temperature for about 30 min, using a mixture of 2% NH_3 in He (75 mL/min), and purged in pure N_2 (75 mL/min) for 4 h to remove all loosely bound NH_3, until no further weight changes were observed. The desorption of NH_3 was then monitored by the weight loss while increasing the temperature to 873 K with 10 K/min in a flow of 75 mL/min N_2.

The FTIR measurements to characterize the Brønsted sites, silanol groups, and other defects in the zeolite material were performed on a Nicolet 6700 FTIR spectrometer, operating in transmission mode at 2 cm^{-1} resolution on self supported pellets. Prior to measurements, the samples were pre-treated at 773 K at $p \leq 1 \times 10^{-4}$ mbar for 1 h. The differences in acid strength and distribution of the different surface hydroxyl groups were derived from the changes in IR absorption of CO probe molecules adsorbed at ~100 K and a partial pressure of 70 mbar. In order to have the possibility to compare band intensities within the full set of spectra, spectra have been normalized to the pellet thickness.

2.3. Studies of catalytic activity

The catalytic activity and deactivation rate for the conversion of methanol to hydrocarbons were determined from the measured hydrocarbon yield with time on stream at constant flow, pressure, and temperature. The measurements were performed in a parallel reactor setup consisting of 10 parallel reactor channels, in which each channel is exposed to the same reaction feed gas at the same reaction conditions. Each reactor channel was filled with a 150 mg sample of the catalyst (sieve fraction 150–300 μm) and exposed to a feed of 14.2% methanol in N_2 at 623 K and 15 bar, using a total flow of 350 N mL/min, which resulted in a flow of 35 N mL/min in each individual reactor channel. These conditions correspond to a WHSV of about 3 g_{MeOH}/g_{cat} h. The reactor exit gas was analyzed by sequentially connecting the individual reactor channels to a mass spectrometer (Balzers GAM 400 or Balzers ThermoStar) *via* a 12 ports channel selection valve. The conversion (hydrocarbon yield) in the reaction exit gas was determined by following $m/e = 32$ (methanol) and $m/e = 46$ (DME) signals with time. The data were analyzed according to the deactivation model discussed by Janssens [60]. In this model, it is assumed that deactivation can be described as a reduction in the effective amount of catalyst with time on stream and that the reaction is first order in methanol. This allows straightforward determination of a rate constant that describes the catalyst activity and a deactivation coefficient. For active catalysts (initial conversion 100%), this coefficient is inversely related to the more familiar conversion capacity in units of grams methanol converted per gram catalyst [60].

3. Results and discussion

As mentioned in Section 1, the exact effects of the desilication procedure are difficult to predict and appear to depend on, among other things, the chemical nature of base employed, the concentration of base, the catalyst to base ratio, the Si/Al ratio of the sample, the crystal size, and the crystal morphology. This complexity and interdependency of parameters often lead to results that in our experience may be perceived as erratic or confusing. During the course of our work on desilication of ZSM-5, we have created, characterized, and investigated the catalytic properties in the conversion of methanol to hydrocarbons (MTH) of a multitude of samples, and based on this experience some fairly evident features have been identified. In this report, we will focus on three sets of parent and desilicated ZSM-5, as well as one mesoporous sample prepared by carbon templating. The results from N_2 sorption experiments and approximate particle sizes are listed in Table 1, Si/Al ratios as determined by ICP and TPD in Table 2, and parameters related to catalyst performance in Table 3. The commercial *c*-ZSM-5 sample displays fairly small particles, a Si/Al close to the optimum for efficient desilication (25–50) as identified by Groen and co-workers, and an intermediate conversion capacity for the parent sample. Sample *h*-ZSM-5 is synthesized in house and has similar particle size and Si/Al ratio to *c*-ZSM-5 and a moderate conversion capacity for the parent sample. Sample *h*-ZSM-5-*xl* is also

Table 1
Particle sizes and textural properties from N_2 adsorption.

Catalyst	Crystal size (μm)	Surface area (m^2/g)	V_{micro} (mL/g)	S_{meso} (m^2/g)
c-ZSM-5	0.5–3	389	0.11	177
c-ZSM-5-*at*		483	0.11	275
h-ZSM-5	0.5–1.5	373	0.14	109
h-ZSM-5-*at*		473	0.10	269
h-ZSM-5-*xl*	15–20	347	0.10	146
h-ZSM-5-*xl*-*at*		431	0.10	243
h-ZSM-5-*ct*	1–5	395	0.09	215

Table 2
Aluminum content and distribution from ICP and NH_3-TPD-TGA.

Catalyst	Si/Al ratio ICP	Si/Al ratio NH_3-TPD-TGA	NH_3 desorption below 350 °C (%)	NH_3 desorption above 350 °C (%)
c-ZSM-5	54	50	38	62
c-ZSM-5-*at*	19	33	50	50
h-ZSM-5	45	47	37	63
h-ZSM-5-*at*	20	40	53	47
h-ZSM-5-*xl*	39	Not available	–	–
h-ZSM-5-*xl*-*at*	28	35	53	47
h-ZSM-5-*ct*	39	65	48	52

Table 3
Activity and deactivation parameters for the conversion of methanol to hydrocarbons.

Catalyst	Conversion capacity (g_{MeOH}/g_{cat})	Activity (mol_{MeOH}/g_{cat} h)	Deactivation (mg_{cat}/mol_{MeOH})
c-ZSM-5	341	43.1	13.3
c-ZSM-5-*at*	1224	14.4	3.6
h-ZSM-5	291	11.6	15.6
h-ZSM-5-*at*	1104	9.9	4.1
h-ZSM-5-*xl*	340	7.0	13.6
h-ZSM-5-*xl*-*at*	876	5.5	5.2
h-ZSM-5-*ct*	581	13.3	7.8

synthesized in-house and comprises very large particles. It is otherwise similar to the *h*-ZSM-5 sample with respect to Si/Al ratio and catalytic properties.

3.1. What is the mode of mesopore formation?

Two modes of mesopore formation upon desilication have been proposed, as outlined above. First, Groen and co-workers have demonstrated that siliceous areas of the zeolite particles may be selectively dissolved, and this is apparently controlled by the distribution of trivalent framework atoms, in effect the Si/Al ratio [7]. Second, Ogura et al. have emphasized the potential importance of dissolution along boundaries or defects within each particle [41]. In this section, we will focus on the commercial ZSM-5 sample (*c*-ZSM-5-*at*) and its desilicated counterpart (*c*-ZSM-5-*at*). In Fig. 1, we display TEM images of *c*-ZSM-5-*at* at increasing magnification. Clearly, mesopores formed according to both proposals are present. We interpret the bright, near circular areas as the removal of siliceous areas. Very similar features have also been observed in other TEM studies of desilicated zeolites [14,26,32,37,39,61–69]. In addition, the formation of radial channels is clearly distinguishable, which we consider to have been formed along the aforementioned defects or boundaries within each particle. Similar phenomena observed by other techniques have previously been referred to by Kox et al. [56] as mesopore "superhighways". Both panels of Fig. 1 display such mesopores, and this is a general feature for the zeolite particles of this sample (not explicitly shown). Typically, many "superhighways" are created within a single particle. These images lead us to the conclusion that both modes of mesopore formation suggested in the literature are active and will to some extent influence the outcome of any desilication procedure.

At this point, a brief discussion of MFI crystal morphology is warranted. Fig. 2 is a collection of SEM micrographs showing some of the crystal habits commonly encountered. Panel A of Fig. 2 is an example of the archetype MFI morphology, often described as twinned prisms. The particles shown in panel B of Fig. 2 appear to be less complex, appearing as smooth and "coffin" shaped without the side protrusions seen in panel A. It should be noted, however, that Weckhuysen and co-workers have shown that even as-synthesized particles that appear to be single crystals are composed of a handful of subunits that often, but not always, are fused in a manner leading to the formation of pyramidal boundaries [70]. In panels C and D, on the other hand, the particles appear to have considerable surface roughness or structure. This is so pronounced in panel D that the typical MFI morphology is hardly discernible. It is straightforward to speculate that particles of such a complex morphology might

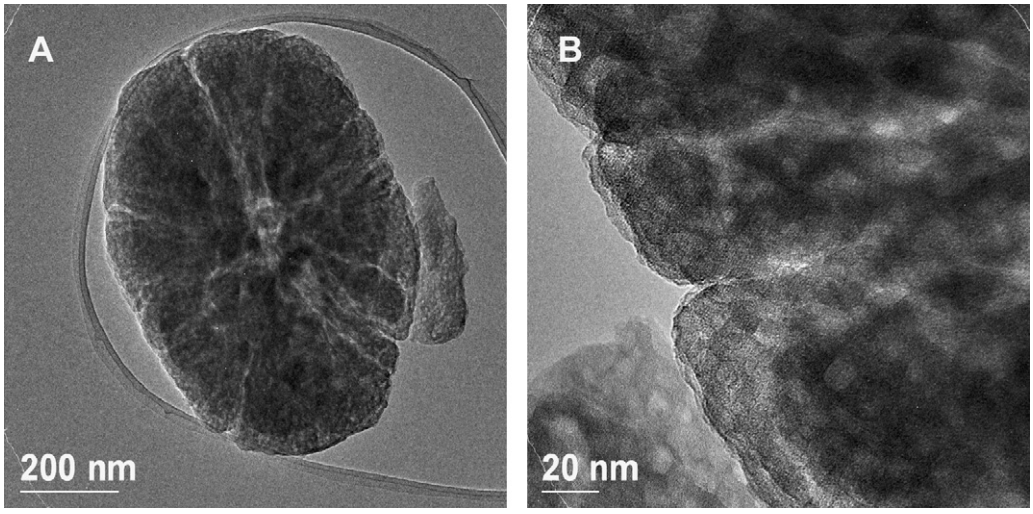

Fig. 1. Representative TEM images of desilicated ZSM-5 (*c*-ZSM-5-*at*).

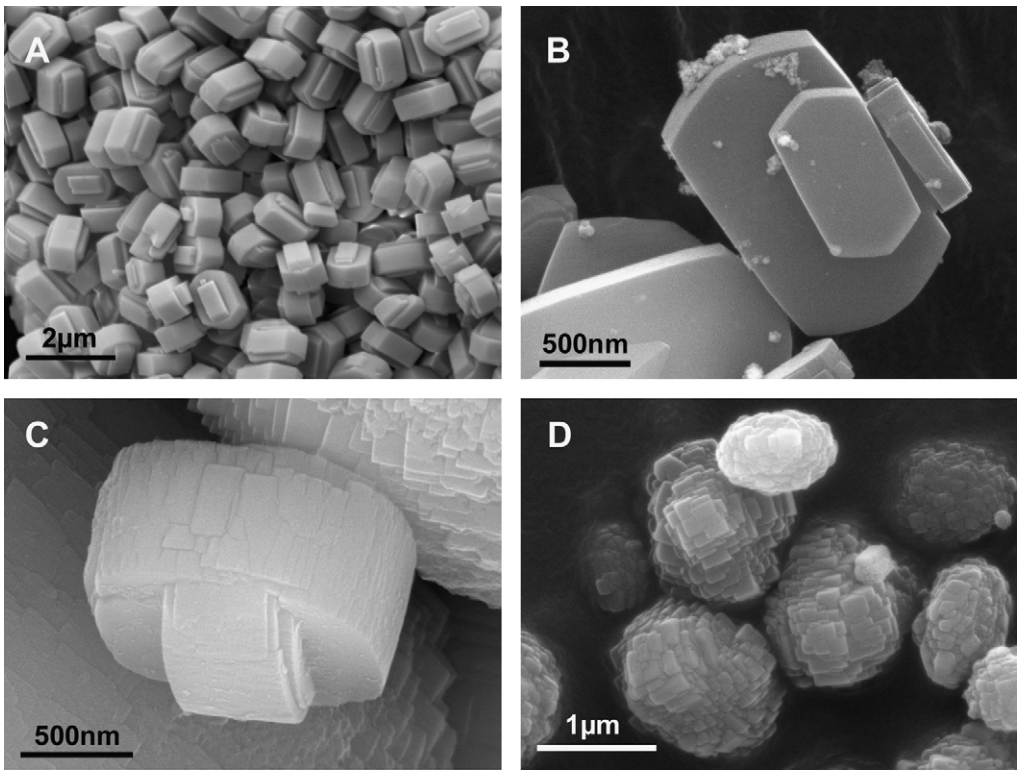

Fig. 2. SEM micrographs showing various ZSM-5 morphologies. Note the differences in magnification.

actually be formed by the fusion of a multitude of smaller, possibly primary crystallites. Similarly, Hayasaka et al. have demonstrated that the crystallization of zeolite ZSM-22 is a two step process, comprising the formation of nanorods that are subsequently aligned and fused through their lateral surfaces, which are Al enriched [71]. Such phenomena are also well known for non-zeolitic materials. In an inspiring review, Imai and Oaki have shown how similar multilevel hierarchies of lengths from nanometers to millimetres are commonly observed in the sophisticated architectures of carbonate based biominerals. These authors refer to these superstructures as mesocrystals, composed of crystallograpically oriented crystals, formed by self organized growth [72].

Based on these perspectives with respect to crystal (inter)growth and the modes of mesopore formation during desilication, we identify the ZSM-5 morphology shown in panels C and D of Fig. 2, where the particles do appear as if they have been formed through the fusion of many smaller units, as the ideal morphology for efficient desilication by the mode proposed by Ogura et al. [41]. This point will be elaborated in the following section.

3.2. The effects of particle size on desilication

SEM images of parent and desilicated ZSM-5 samples are shown in Fig. 3. The pore size distributions are given as insets in each panel, and textural properties are given in Table 1. All three samples consist of particles having the optimum morphology for desilication as discussed in the preceding section. Desilication is thus likely to proceed also according to the mode suggested by Ogura et al. [41]. Indeed, this is partly visible for all samples also when using SEM, albeit not so clearly as demonstrated for the *c*-ZSM-5-*at* sample with TEM in Fig. 1. Panels A and B of Fig. 3 show *c*-ZSM-5 and *c*-ZSM-5-*at* respectively, and will not be discussed further. Panels C and D, on the other hand, show the parent and desilicated versions of *h*-ZSM-5. This material consists of particles of similar size to those seen in *c*-ZSM-5, and efficient desilication is readily achieved. This is straightforwardly seen in the SEM images and the accompanying BJH pore size distribution, as well as from the substantial increase in the external surface area and the profound improvement of the catalytic properties listed in Table 3. The Si/Al ratio as determined by ICP is more than halved as a consequence of the treatment, indicative of extensive dissolution. The influence of zeolite particle size is explored for *h*-ZSM-5-*xl*, which displays the same optimum morphology as *c*-ZSM-5 and *h*-ZSM-5, but consists of very large particles. The SEM images of the parent and desilicated sample in panels E and F of Fig. 3 again show considerable modification of the external particle surface. Also, the reduction in Si/Al ratio and the textural data listed in Table 1 as well as the improvement in catalytic properties (Table 3) point to efficient desilication also of this sample comprising very large particles. It has previously been reported that desilication is inefficient for crystals larger than 3 μm, and it was proposed that this could be due to mass transfer limitations of the desilication process itself or Al gradients leading to more resistant particles [73]. The results presented for *h*-ZSM-5-*xl*-*at* clearly demonstrate that large particles are not intrinsically unsusceptible to desilication, as the increase in the external surface and the improvement of the catalytic properties is comparable to those achieved for the considerable smaller particles of *c*-ZSM-5-*at* and *h*-ZSM-5-*at*. However, a more severe treatment procedure was required to desilicate *h*-ZSM-5-*xl* to an extent comparable to that achieved for *h*-ZSM-5 at milder conditions (see Section 2). Also, it should be kept in mind that our samples all display the complex morphology discussed above, and it appears plausible that the predominant mode of mesopore formation in *h*-ZSM-5-*xl*-*at* is dissolution or etching along boundaries, intergrowths, and defects within each particle.

3.3. The effects of desilication of Al environment, acidity, and catalytic properties

Full NH_3-TPD profiles of all materials except the *h*-ZSM-5-*xl* sample, are given in Fig. 4, and a quantitative analysis of the desorption experiments is listed in Table 2. Clearly, and as mentioned

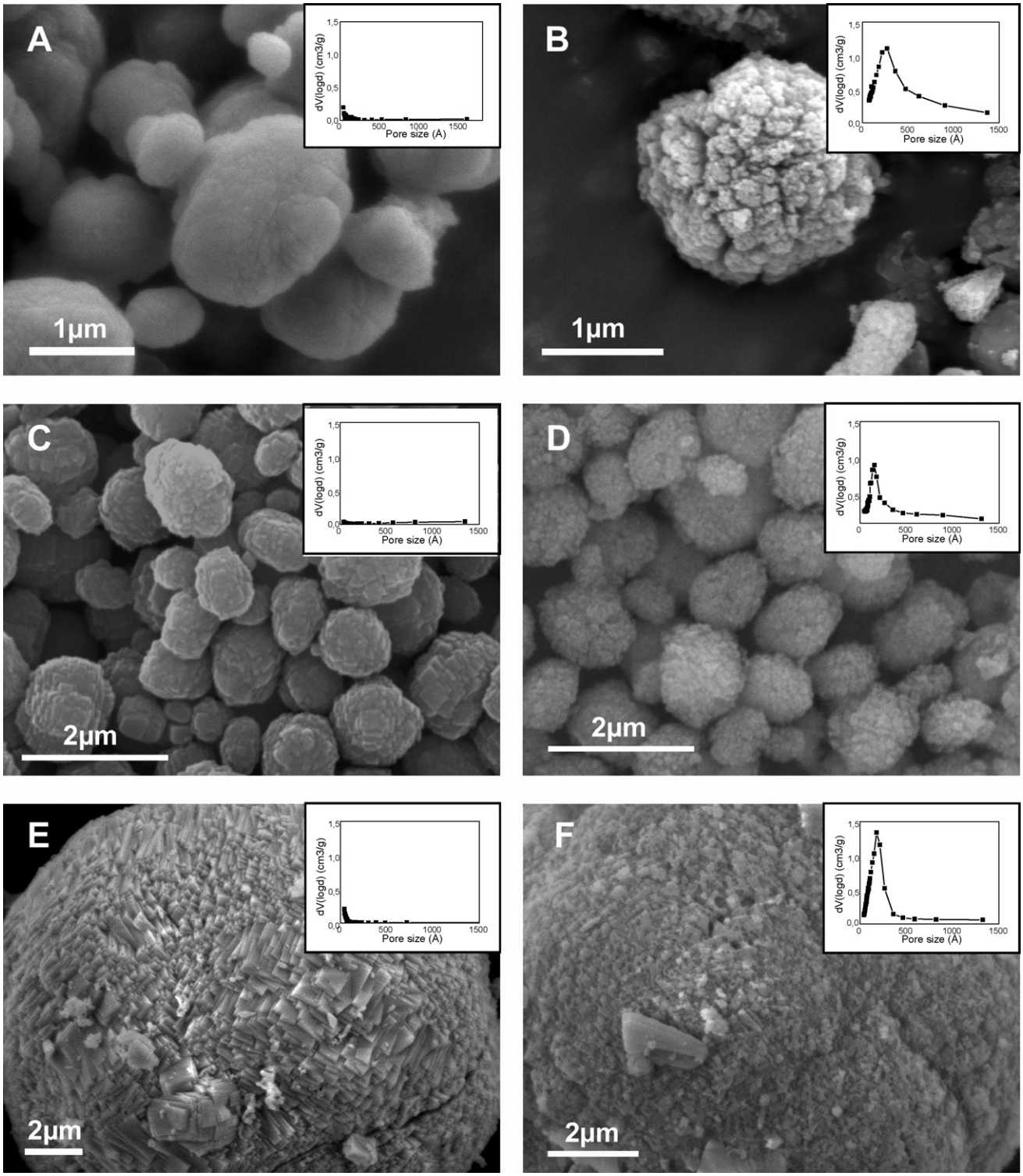

Fig. 3. SEM micrographs and BJH pore size distribution plots for non-treated (left column) and desilicated (right column) ZSM-5. Top row (panels A and B): *c*-ZSM-5 and *c*-ZSM-5-*at*; middle row (panels C and D): *h*-ZSM-5 and *h*-ZSM-5-*at*; bottom row (panels E and F): *h*-ZSM-5-*xl* and *h*-ZSM-5-*xl*-*at*.

above, for all materials, desilication leads to a decrease in the Si/Al as determined by ICP. This is in line with the observations generally reported. Comparison of the ICP values to those determined using NH_3-TPD reveal three general features. First, ICP and TPD agree very well for the parent samples. This implies that virtually all Al atoms occupy tetrahedral framework positions and contribute to strong Brønsted acidity for these unmodified materials. Second, such an agreement is very clearly not found for the desilicated materials; the Si/Al ratios available are in both cases significantly higher in the TPD measurements compared to ICP. This means that a sizeable fraction of the Al does not contribute to any TPD-measurable acidity, in turn suggesting that extra framework Al is formed upon desilication. Third, inspection of the actual TPD profiles in Fig. 4 reveals that the distribution of acid sites also changes considerably upon desilication for the samples presented in this work. It appears that desilication leads to a considerable forma-

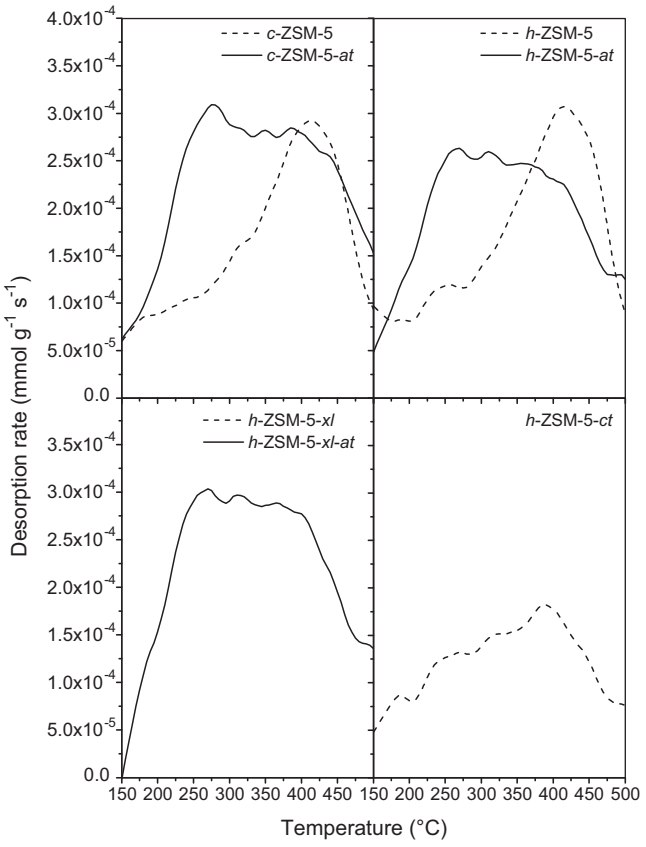

Fig. 4. Temperature programmed desorption of ammonia profiles as determined by means of thermogravimetry.

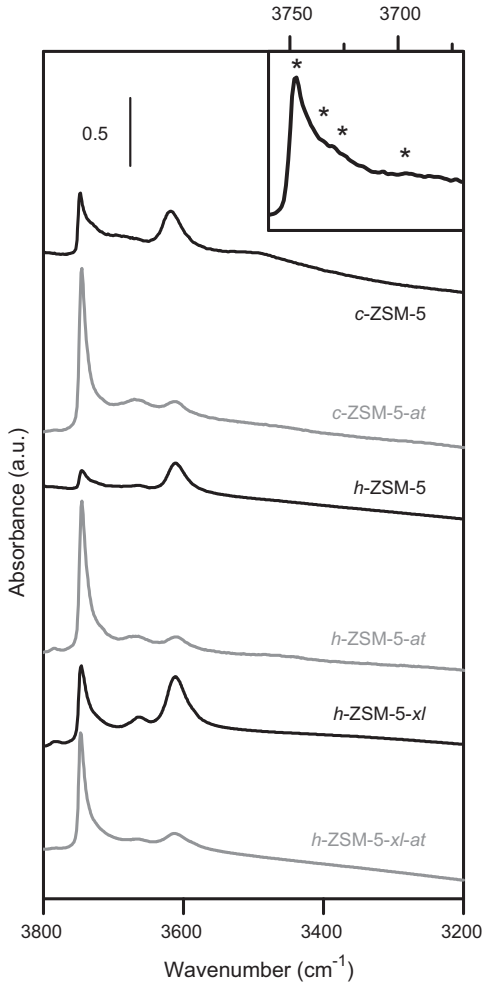

Fig. 5. FTIR spectra of the ν(OH region) for the parent (black spectra) and desilicated (grey spectra) ZSM-5. The inset shows an expanded view of the complex absorption due to isolated and weakly perturbed silanols for the *c*-ZSM-5 sample (up to four components are seen at 3745, 3735, 3726 and 3700 cm^{-1}).

tion of weaker acid sites, as evidenced by significant desorption at fairly low temperatures seen for *c*-ZSM-5-*at* and *h*-ZSM-5-*at*. This is further emphasized in Table 2, where the desorption has been subdivided (somewhat arbitrarily) into a high temperature loss (above 623 K) and low temperature loss (below 623 K). Interestingly, the desorption profiles presented in Fig. 4 are quite different from those presented in some literature reports, wherein the TPD profiles are virtually unaltered after desilication of ZSM-5 samples [18,19]. Others reports do, however, describe an increase in the concentration of weak acid sites and/or a reduction of the strong acid sites [14,23,26,39], suggesting that further systematic studies might be required to determine the cause of such different behaviors.

Complementary information to that obtained by TPD is available by comparing the IR spectra of the activated samples in the hydroxyls stretching region (3800–3200 cm^{-1}) as displayed in Fig. 5. The spectra have been normalized with respect to the pellet thickness, and the band intensities are therefore within reasonable accuracy representative of the amounts of the respective species. Black curves correspond to parent samples, while grey curves refer to desilicated counterparts. All the spectra are characterized by various components for which the relative abundances differ within the series, and in particular: (i) a complex absorption in the range of 3750–3700 cm^{-1} due to isolated and weakly perturbed silanols (composed of up to four contributions at 3745, 3735, 3726 and 3700 cm^{-1}, as highlighted in the inset of Fig. 5); (ii) a component at about 3668 cm^{-1}, ascribed to partial extra-framework Al and (iii) the well known band at 3610 cm^{-1}, corresponding to the Si(OH)Al Brønsted acid sites. Alkali treatment affects the spectra in similar ways (from black to grey curves): (i) the isolated silanol component at 3745 cm^{-1} gains in intensity, while the features at lower frequencies associated to weakly interacting silanols, become less evident; (ii) the Brønsted band at 3610 cm^{-1} tends to decrease, and concurrent formation of entrapped extra-framework Al is observed for the *c*-ZSM-5-*at* and *h*-ZSM-5-*at* samples. In contrast, the parent *h*-ZSM-5-*xl* contained a significant contribution of partial extra-framework Al, of which some is clearly removed upon desilication. These observations agree very well with the information gleaned from NH_3-TPD, and it is tempting to link the appearance of partial extra framework Al seen at 3668 cm^{-1} to the formation of comparatively weak acid sites. Taken together, the features observed both with IR and TPD suggest that for the present set of samples, the alkali treatment does not cause simply a dissolution of the zeolite framework, but also a reorganization of the tetrahedral lattice positions, resulting in (i) an increase in the concentration of isolated silanols, previously suggested to be indicative of mesopore formation [34,74]; (ii) a decrease of defective regions associated to internal hydroxylated nests; (iii) a reduction in the density of strong Brønsted acid sites; (iv) an increased concentration of weak acid sites.

Obviously, the profound changes in both acidic properties and porosity outlined in the preceding paragraphs are expected to influence the catalytic properties of the materials, and this is indeed the case. Catalyst performance in the conversion of methanol to hydrocarbons is summarized in Table 3. Comparison of catalyst performance is a complex issue, but some features appear to be general. First, it appears that desilication leads to a reduced activity. This is

reasonable for the current set of samples, for which a reduction in the density of strong Brønsted acid sites has been demonstrated. Second, a reduction in the magnitude of the deactivation coefficient or, conversely, an increased conversion capacity is always seen after desilication, in agreement with previous reports for the same reaction [34]. The cause of this reduced tendency towards deactivation is probably complex, but two evident causes, in addition to the effects of the changes in acidity outlined above, are fairly straightforward. It has been proposed that mesoporosity leads to enhanced mass transfer of coke precursors [65], or possibly an increased tolerance for coke deposition *i.e.* that a higher coke loading is required to deactivate the catalyst [75]. An alternative or co-contributing cause could be related to the rearrangement of surface hydroxyls seen in the silanol region of the IR spectra: in particular, the abundance of species associated to the IR component at 3726 cm^{-1} has very recently been demonstrated to be detrimental for the catalytic performances of the catalysts [76].

3.4. Carbon-templating versus desilication

As mentioned in Section 1, several synthesis strategies might be followed in order to achieve a material with a hierarchical pore system. Apart from the already described method of desilication *via* base treatment, the carbon templating method has been reported in many occasions to result in hierarchical zeolites with improved catalytic properties [7,77–79]. From a practical point of view, the carbon templating method clearly is more time consuming and requires more preparative steps to achieve the desired hierarchical material, *i.e.* when compared to desilication *via* base treatment. On the other hand, the carbon templating method can be applied to a wide range of zeolite materials; it is largely independent of the Si/Al ratio of final material; and extensive material loss through dissolution is not an issue.

Regardless of the practical aspects of the two approaches, the more important question is if the mesopores created *via* the two different methods, are essentially comparable or if there are substantial differences between them. Several authors have addressed this question [65,80]. Mei et al. compared desilicated ZSM-5 to samples where the mesoporosity was introduced by using starch as a soft template and found that the mesopores thus created were located predominantly inside the zeolite body and played a limited role in the diffusion of gas molecules and had little effect on the catalytic performance [80]. Also, Kim et al. have compared mesoporous ZSM-5 samples made by using organosilane surfactants to catalysts prepared by desilication and carbon templating [65]. We have prepared a carbon templated sample (*h*-ZSM-5-*ct*), with the aim of comparing it to the home-made, alkali treated sample (*h*-ZSM-5-*at*). The SEM image shown in Fig. 6 confirms that a rather similar particle size and morphology was achieved. Even though the total surface and mesopore surface area of *h*-ZSM-5-*at* are somewhat higher compared to *h*-ZSM-5-*ct* (Table 1), the overall textural properties of the two samples appear rather similar, facilitating a comparison between them.

In Fig. 7 the IR spectra of *h-ZSM-5-at* (top) and *h-ZSM-5-ct* (bottom) are shown, before (dashed dotted curves) and after CO adsorption (full line curves). Note that for both samples, significant amounts of extra-framework Al are evidenced in the spectra (band at 3668 and 3785 cm^{-1}). This is also reflected in the shape of the NH_3-TPD desorption curves, which suggest a significant amount of weak acid sites also in the carbon templated material. The most striking difference between the two catalysts, however, is evident in the range of the silanol groups (3700–3750 cm^{-1}). The IR spectrum of the *h-ZSM-5-ct* sample shows considerable components at 3700 and 3726 cm^{-1}, indicating a high amount of internal defects compared to *h-ZSM-5-at*. This is significant, as a correlation between defects located in the micropores of ZSM-5 and the

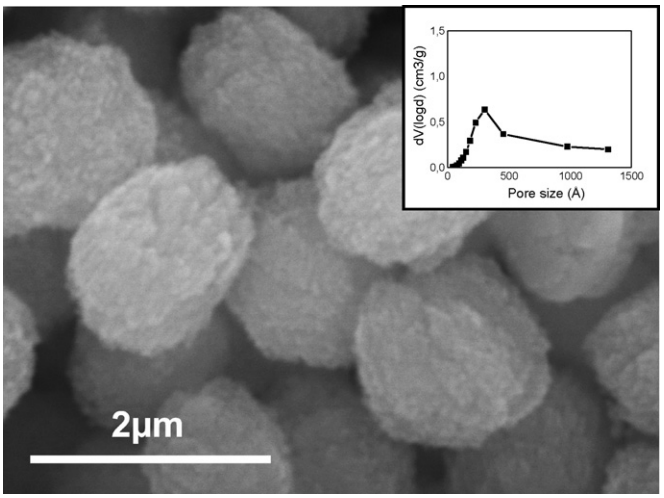

Fig. 6. SEM micrograph and BJH pore size distribution plot for carbon-templated ZSM-5 (*h*-ZSM-5-*ct*).

deactivation rate of the catalyst during MTG reaction recently has been established [76]. Indeed, the parameters related to catalytic performance listed in Table 3 show that the desilicated sample outperforms the carbon templated catalyst with respect to conversion capacity (or slow deactivation), although not dramatically. Both the analyses of Al content and distribution (Table 2) and the intensity of the Brønsted band at 3610 cm^{-1} indicate that the concentration of strong acid sites is somewhat smaller in the carbon templated sample. However, this is not reflected in a lower activity for *h*-ZSM-5-*ct* sample, as one might have expected. This emphasizes the complexity of comparing the catalytic performance of samples of widely different preparation and treatment procedures.

The acid strength of the surface hydroxyls was explored by CO adsorption at low temperature (Fig. 7). Both samples show very similar behavior for the components at 3668 and 3610 cm^{-1}, which are shifted to 3460 and 3290 cm^{-1} respectively. In parallel, in the CO stretching frequency region (Fig. 7b), an asymmetric maxima at 2175 cm^{-1}, with a shoulder at 2170 cm^{-1} is observed. Differences

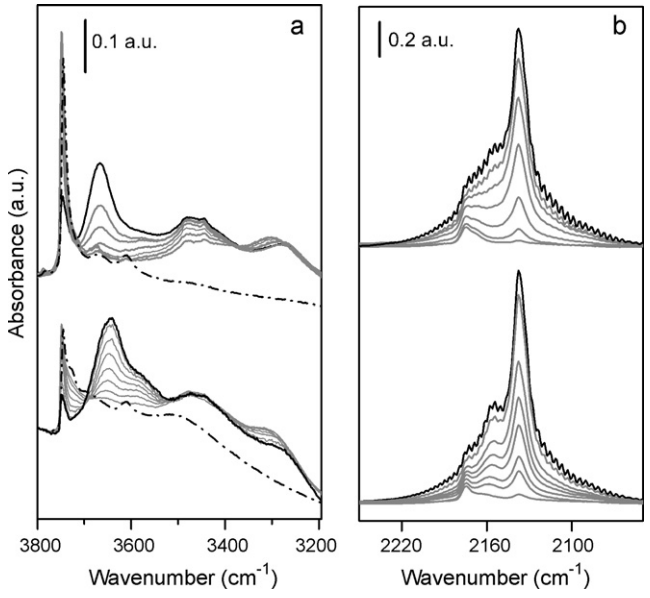

Fig. 7. FTIR spectra of progressive CO coverages on: *h*-ZSM-5-*at* (top); *h*-ZSM-5-*ct* (bottom); part (a) ν(OH); part (b) ν(CO) after background subtraction; zeolites background spectra: dot dashed lines; effect of maximum CO coverages: black full lines; intermediate CO coverages: grey lines.

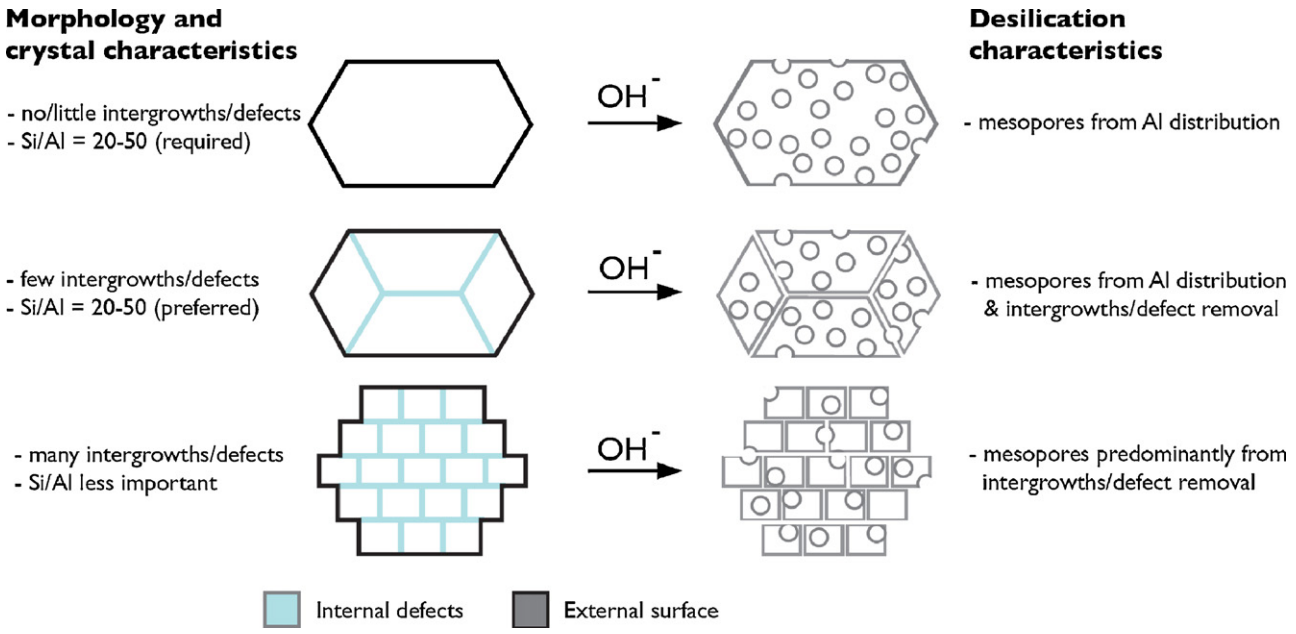

Fig. 8. Schematic representation of different idealized mesopore formation mechanisms.

are, however, observed in the silanol regions upon adsorption of CO. For both samples, not all silanols are eroded upon CO interaction. Apparently, not all these surface hydroxyls are available for molecules diffusing into the catalyst particles from the gas phase. This feature is most pronounced for the desilicated samples, and conversely, the silanols of *h-ZSM-5-ct* are considerably more extensively engaged. The components at 3726 and at 3700 cm^{-1} (only clearly visible in case of *h-ZSM-5-ct*), are readily eroded giving rise to a pronounced broad band with a maximum at 3650 cm^{-1} extending to 3530 cm^{-1}. The spectra associated to the *h-ZSM-5-at* sample show a more symmetric band centered at 3670 cm^{-1}. In the CO stretching region of *h-ZSM-5-ct*, a distinct band is observed at 2156 cm^{-1}, while for *h-ZSM-5-at*, at the same position an unstructured broad absorption is monitored. The observed features in the CO adsorption spectra reveal that *h-ZSM-5-ct* is characterized by an unusual distribution of surface sites and acidity caused by a high amount of internal silanols.

It is evident from these results that hierarchical zeolites with similar textural properties and Brønsted acid site densities can have significantly different surface properties depending on the chosen synthetic approach. In our case, the carbon templating method resulted in a material with a high concentration and wide distribution of surface hydroxyls/defects. An explanation for this high amount of internal silanols could be given by considering the relative high local temperature peaks during the combustion of the carbon template *via* calcination. Therefore, care should be taken when removing the hard template, to avoid damaging the zeolite structure, which might decrease the beneficial effects of mesopores for catalytic applications. These observations straightforwardly lead to the notion of combining carbon templating and desilication, and this has already been demonstrated to be highly efficient [81].

4. Summary and conclusions

In this contribution, we have addressed the mode of mesopore formation in ZSM-5 by desilication, which is a simple and fast method to introduce mesoporosity leading to improved catalyst performance. Mesopore formation according to both Al-directed dissolution of siliceous areas and selective dissolution or etching along boundaries, intergrowths, and defects within each particle are important. Fig. 8 gives a schematic overview of the different mesopores and their formation mechanism. This realization has allowed us to identify a preferred particle morphology for efficient desilication of ZSM-5, as particles constructed of fused subunits appear to be very susceptible towards directed mesopore formation by desilication, irrespective of particle size. Moreover, FTIR and NH_3-TPD have revealed that the concentration and distribution of surface hydroxyls associated to various silanols, partially extra-framework Al, and Brønsted sites may be strongly influence by desilication. A tendency for a reduction in the concentration of strong Brønsted sites and concurrent formation of weaker acid sites has been demonstrated. This leads to a somewhat lower catalytic activity in the conversion of methanol to hydrocarbons, but desilication also causes a substantially improved resistance towards deactivation. Carbon templating tends to lead to a more defect rich mesoporous material than desilication. Nevertheless, improved performance in the MTH reaction is observed for catalysts prepared by both methods, although we emphasize that the comparison of catalyst performance between (mesoporous) samples of ZSM-5 prepared by different routes is not straightforward, as the Si/Al ratio, distribution of defects observable with FTIR, mesoporosity, particle size and other characteristics will influence activity and deactivation rates in an interdependent manner.

Acknowledgement

This publication forms a part of the inGAP Center of Research-based Innovation, which receives financial support from the Research Council of Norway under contract no. 174893.

References

[1] W. Vermeiren, J.P. Gilson, Top. Catal. 52 (2009) 1131–1161.
[2] J. Coronas, Chem. Eng. J. 156 (2010) 236–242.
[3] J.X. Jiang, J.H. Yu, A. Corma, Angew. Chem. Int. Ed. 49 (2010) 3120–3145.
[4] M. Moliner, M.J. Diaz-Cabanas, V. Fornes, C. Martinez, A. Corma, J. Catal. 254 (2008) 101–109.
[5] L. Tosheva, V.P. Valtchev, Chem. Mater. 17 (2005) 2494–2513.
[6] M. Hartmann, Angew. Chem. Int. Ed. 43 (2004) 5880–5882.
[7] J. Perez-Ramirez, C.H. Christensen, K. Egeblad, C.H. Christensen, J.C. Groen, Chem. Soc. Rev. 37 (2008) 2530–2542.

[8] S. van Donk, A.H. Janssen, J.H. Bitter, K.P. de Jong, Catal. Rev. Sci. Eng. 45 (2003) 297–319.
[9] K. Egeblad, C.H. Christensen, M. Kustova, C.H. Christensen, Chem. Mater. 20 (2008) 946–960.
[10] R. Le Van Mao, S.Y. Xiao, A. Ramsaran, J.H. Yao, J. Mater. Chem. 4 (1994) 605–610.
[11] R. Le Van Mao, A. Ramsaran, S. Xiao, J. Yao, V. Semmer, J. Mater. Chem. 5 (1995) 533–535.
[12] R. Le Van Mao, S.T. Le, D. Ohayon, F. Caillibot, L. Gelebart, G. Denes, Zeolites 19 (1997) 270–278.
[13] M. Ogura, S. Shinomiya, J. Tateno, Y. Nara, M. Nomura, E. Kikuchi, M. Matsukata, Chem. Lett. 8 (2000) 882.
[14] M. Ogura, S. Shinomiya, J. Tateno, Y. Nara, M. Nomura, E. Kikuchi, M. Matsukata, Appl. Catal. A 219 (2001) 33–43.
[15] J.C. Groen, L.A.A. Peffer, J.A. Moulijn, J. Perez-Ramirez, Colloid Surf. A: Physicochem. Eng. Aspects 241 (2004) 53–58.
[16] J.C. Groen, J.C. Jansen, J.A. Moulijn, J. Perez-Ramirez, J. Phys. Chem. B 108 (2004) 13062–13065.
[17] J.C. Groen, T. Bach, U. Ziese, A.M. Paulaime-van Donk, K.P. de Jong, J.A. Moulijn, J. Perez-Ramirez, J. Am. Chem. Soc. 127 (2005) 10792–10793.
[18] J.C. Groen, J.A. Moulijn, J. Perez-Ramirez, Micropor. Mesopor. Mater. 87 (2005) 153–161.
[19] J.C. Groen, L.A.A. Peffer, J.A. Moulijn, J. Perez-Ramirez, Chem. Eur. J. 11 (2005) 4983–4994.
[20] J.C. Groen, J.A. Moulijn, J. Perez-Ramirez, J. Mater. Chem. 16 (2006) 2121–2131.
[21] J.C. Groen, J.A. Moulijn, J. Perez-Ramirez, Ind. Eng. Chem. Res. 46 (2007) 4193–4201.
[22] J.C. Groen, L.A.A. Peffer, J.A. Moulijn, J. Perez-Ramirez, Micropor. Mesopor. Mater. 69 (2004) 29–34.
[23] J.C. Groen, T. Sano, J.A. Moulijn, J. Perez-Ramirez, J. Catal. 251 (2007) 21–27.
[24] J.C. Groen, S. Abello, L.A. Villaescusa, J. Perez-Ramirez, Micropor. Mesopor. Mater. 114 (2008) 93–102.
[25] X.F. Li, R. Prins, J.A. van Bokhoven, J. Catal. 262 (2009) 257–265.
[26] A. Bonilla, D. Baudouin, J. Perez-Ramirez, J. Catal. 265 (2009) 170–180.
[27] X.T. Wei, P.G. Smirniotis, Micropor. Mesopor. Mater. 97 (2006) 97–106.
[28] A. van Miltenburg, J. Pawlesa, A.M. Bouzga, N. Zilkova, J. Cejka, M. Stöcker, Top. Catal. 52 (2009) 1190–1202.
[29] J. Perez-Ramirez, S. Abello, L.A. Villaescusa, A. Bonilla, Angew. Chem. Int. Ed. 47 (2008) 7913–7917.
[30] L. Sommer, D. Mores, S. Svelle, M. Stöcker, B.M. Weckhuysen, U. Olsbye, Micropor. Mesopor. Mater. 132 (2010) 384–394.
[31] V. Paixão, A.P. Carvalho, J. Rocha, A. Fernandes, A. Martins, Micropor. Mesopor. Mater. 131 (2010) 350–357.
[32] D. Verboekend, L.A. Villaescusa, K. Thomas, I. Stan, J. Perez-Ramirez, Catal. Today 152 (2010) 11–16.
[33] C.S. Mei, Z.C. Liu, P.Y. Wen, Z.K. Xie, W.M. Hua, Z. Gao, J. Mater. Chem. 18 (2008) 3496–3500.
[34] M. Bjørgen, F. Joensen, M.S. Holm, U. Olsbye, K.P. Lillerud, S. Svelle, Appl. Catal. A 345 (2008) 43–50.
[35] X. Gao, Z. Tang, G. Lu, G. Cao, D. Li, Z. Tan, Solid State Sci. 12 (2010) 1278–1282.
[36] B. Gil, L. Mokrzycki, B. Sulikowski, Z. Olejniczak, S. Walas, Catal. Today 152 (2010) 24–32.
[37] S. Abello, A. Bonilla, J. Perez-Ramirez, Appl. Catal. A 364 (2009) 191–198.
[38] M.S. Holm, M.K. Hansen, C.H. Christensen, Eur. J. Inorg. Chem. 9 (2009) 1194–1198.
[39] R. Caicedo-Realpe, J. Perez-Ramirez, Micropor. Mesopor. Mater. 128 (2010) 91–100.
[40] A. Ciziek, B. Subotic, I. Smit, A. Tonejc, R. Aiello, F. Crea, A. Nastro, Micropor. Mater. 8 (1997) 159–169.
[41] M. Ogura, E. Kikuchi, M. Matsukata, Stud. Surf. Sci. Catal. 135 (2001) 216–223.
[42] G. Müller, T. Narbeshubert, G. Mirth, J.A. Lercher, J. Phys. Chem. 98 (1994) 7436–7439.
[43] P. Kortunov, S. Vasenkov, C. Chmelik, J. Kärger, D.M. Ruthven, J. Wloch, Chem. Mater. 16 (2004) 3552–3558.
[44] O. Geier, S. Vasenkov, E. Lehmann, J. Kärger, U. Schemmert, R.A. Rakoczy, J. Weitkamp, J. Phys. Chem. B 105 (2001) 10217–10222.
[45] D. Tzoulaki, L. Heinke, W. Schmidt, U. Wilczok, J. Kärger, Angew. Chem. Int. Ed. 47 (2008) 3954–3957.
[46] M.B.J. Roeffaers, R. Ameloot, A.J. Bons, W. Mortier, G. De Cremer, R. de Kloe, J. Hofkens, D.E. De Vos, B.F. Sels, J. Am. Chem. Soc. 130 (2008) 13516–13517.
[47] M.B.J. Roeffaers, R. Ameloot, M. Baruah, H. Uji-i, M. Bulut, G. De Cremer, U. Müller, P.A. Jacobs, J. Hofkens, B.F. Sels, D.E. De Vos, J. Am. Chem. Soc. 130 (2008) 5763–5772.
[48] L. Karwacki, E. Stavitski, M.H.F. Kox, J. Kornatowski, B.M. Weckhuysen, Angew. Chem. Int. Ed. 46 (2007) 7228–7231.
[49] M.W. Anderson, K.S. Pachis, F. Prebin, S.W. Carr, O. Terasaki, T. Ohsuna, V. Alfreddson, J. Chem. Soc., Chem. Commun. (1991) 1660–1664.
[50] M. Pan, Micron 27 (1996) 219–238.
[51] G. Gonzalez, W. Stracke, Z. Lopez, U. Keller, A. Ricker, R. Reichelt, Microsci. Microanal. 10 (2004) 224–235.
[52] M.W. Anderson, J.R. Agger, L.I. Meza, C.B. Chong, C.S. Cundy, Faraday Discuss. 136 (2007) 143–156.
[53] L. Brabec, M. Kocirik, Mater. Chem. Phys. 102 (2007) 67–74.
[54] E. Stavitski, M.H.F. Kox, B.M. Weckhuysen, Chem. Eur. J. 13 (2007) 7057–7065.
[55] M.H.F. Kox, E. Stavitski, B.M. Weckhuysen, Angew. Chem. Int. Ed. 46 (2007) 3652–3655.
[56] M.H.F. Kox, E. Stavitski, J.C. Groen, J. Perez-Ramirez, F. Kapteijn, B.M. Weckhuysen, Chem. Eur. J. 14 (2008) 1718–1725.
[57] E. Stavitski, M.H.F. Kox, I. Swart, F.M.F. de Groot, B.M. Weckhuysen, Angew. Chem. Int. Ed. 47 (2008) 3543–3547.
[58] P.N.R. Vennestrøm, M. Grill, M. Kustova, K. Egeblad, L.F. Lundegaard, F. Joensen, C.H. Christensen, P. Beato, Hierarchical ZSM-5 prepared by guanidinium base treatment: understanding microstructural characteristics and impact on MTG and NH_3–SCR catalytic reactions, Catal. Today, in press.
[59] M. Kustova, A.L. Kustov, C.H. Christensen, Stud. Surf. Sci. Catal. 158 (2005) 255–262.
[60] T.V.W. Janssens, J. Catal. 264 (2009) 130–137.
[61] S. Abello, J. Perez-Ramirez, Phys. Chem. Chem. Phys. 11 (2009) 2959–2963.
[62] N. Danilina, F. Krumeich, J.A. van Bokhoven, J. Catal. 272 (2010) 37–43.
[63] C. Fernandez, I. Stan, J.P. Gilson, K. Thomas, A. Vicente, A. Bonilla, J. Perez-Ramirez, Chem. Eur. J. 16 (2010) 6224–6233.
[64] J.C. Groen, R. Caicedo-Realpe, S. Abellp, J. Perez-Ramirez, Mater. Lett. 63 (2009) 1037–1040.
[65] J. Kim, M. Choi, R. Ryoo, J. Catal. 269 (2010) 219–228.
[66] J. Perez-Ramirez, D. Verboekend, A. Bonilla, S. Abello, Adv. Funct. Mater. 19 (2009) 3972–3979.
[67] F. Thibault-Starzyk, I. Stan, S. Abello, A. Bonilla, K. Thomas, C. Fernandez, J.P. Gilson, J. Perez-Ramirez, J. Catal. 264 (2009) 11–14.
[68] D. Verboekend, J.C. Groen, J. Perez-Ramirez, Adv. Funct. Mater. 20 (2010) 1441–1450.
[69] D. Verboekend, R. Caicedo-Realpe, A. Bonilla, M. Santiago, J. Perez-Ramirez, Chem. Mater. 22 (2010) 4679–4689.
[70] L. Karwacki, M.H.F. Kox, D.A.M. deWinter, M.R. Drury, J.D. Meeldijk, E. Stavitski, W. Schmidt, M. Mertens, P. Cubillas, N. John, A. Chan, N. Kahn, S.R. Bare, M. Anderson, J. Kornatowski, B.M. Weckhuysen, Nat. Mater. 8 (2009) 959–965.
[71] K. Hayasaka, D. Liang, W. Huybrechts, B.R. De Waele, K.J. Houthoofd, P. Eloy, E.M. Gaigneaux, G. van Tendeloo, J.W. Thybaut, G.B. Marin, J.F.M. Denayer, G.V. Baron, P.A. Jacobs, C.E.A. Kirschhock, J.A. Martens, Chem. Eur. J. 13 (2007) 10070–10077.
[72] H. Imai, Y. Oaki, Mater. Res. Soc. Bull. 35 (2010) 138–144.
[73] J.C. Groen, L.A.A. Peffer, J.A. Moulijn, J. Perez-Ramirez, Stud. Surf. Sci. Catal. 156 (2005) 401–408.
[74] M.S. Holm, S. Svelle, F. Joensen, P. Beato, C.H. Christensen, S. Bordiga, M. Bjørgen, Appl. Catal. A 356 (2009) 23–30.
[75] M. Choi, K. Na, J. Kim, Y. Sakamoto, O. Terasaki, R. Ryoo, Nature 461 (2009) 246–250.
[76] P. Beato, Patent No. WO 2010099885 (2010).
[77] I. Schmidt, A. Krogh, K. Wienberg, A. Carlsson, M. Brorson, C.J.H. Jacobsen, Chem. Commun. 21 (2000) 2157–2158.
[78] C.H. Christensen, I. Schmidt, C.H. Christensen, Catal. Commun. 5 (2004) 543–546.
[79] M. Yu, S.B. Kustova, A.L. Rasmussen, C.H. Kustov, Christensen, Appl. Catal. B 67 (2006) 60–67.
[80] C. Mei, P. Wen, Z. Liu, H. Liu, Y. Wang, W. Yang, Z. Xie, W. Hua, Z. Gao, J. Catal. 258 (2008) 243–249.
[81] M.S. Holm, K. Egeblad, P.N.R. Vennestrøm, C.G. Hartmann, M. Kustova, C.H. Christensen, Eur. J. Inorg. Chem. (2008) 5185–5189.